CM^2 Magazine

第 130 期

南方科技大学海洋磁学中心主编

https://cm2.sustech.edu.cn/

创刊词

海洋是生命的摇篮，是文明的纽带。地球上最早的生命诞生于海洋，海洋里的生命最终进化成了人类，人类的文化融合又通过海洋得以实现。人因海而兴。

人类对海洋的探索从未停止。从远古时代美丽的神话传说，到麦哲伦的全球航行，再到现代对大洋的科学钻探计划，海洋逐渐从人类敬畏崇拜幻想的精神寄托演变成可以开发利用与科学研究的客观存在。其中，上个世纪与太空探索同步发展的大洋科学钻探计划将人类对海洋的认知推向了崭新的纬度：深海（deep sea）与深时（deep time）。大洋钻探计划让人类知道，奔流不息的大海之下，埋藏的却是亿万年的地球历史。它们记录了地球板块的运动，从而使板块构造学说得到证实；它们记录了地球环境的演变，从而让古海洋学方兴未艾。

在探索海洋的悠久历史中，从大航海时代的导航，到大洋钻探计划中不可或缺的磁性地层学，磁学发挥了不可替代的作用。这不是偶然，因为从微观到宏观，磁性是最基本的物理属性之一，可以说，万物皆有磁性。基于课题组的学科背景和对海洋的理解，我们对海洋的探索以磁学为主要手段，海洋磁学中心因此而生。

海洋磁学中心，简称 CM^2，一为其全名“Centre for Marine Magnetism”的缩写，另者恰与爱因斯坦著名的质能方程 $E = MC^2$ 对称，借以表达我们对科学巨匠的敬仰和对科学的不懈追求。

然而科学从来不是单打独斗的产物。我们以磁学为研究海洋的主攻利器，但绝不仅限于磁学。凡与磁学相关的领域均是我们关注的重点。为了跟踪反映国内外地球科学特别是与磁学有关的地球科学领域的最新研究进展，海洋磁学中心特地主办 CM^2 Magazine，以期与各位地球科学工作者相互交流学习、合作共进！

“海洋孕育了生命，联通了世界，促进了发展”。21 世纪是海洋科学的时代，由陆向海，让我们携手迈进中国海洋科学的黄金时代。

目 录

1. 20 世纪的快速变暖逆转了缅因洲海湾 900 年来变冷

翻译人：仲义 zhongy@sustech.edu.cn

Whitney, N.M., Wanamaker, A.D., Ummenhofer, C.C., et al., ***Rapid 20th century warimg reverses 900-year cooling in the Gulf of Maine*** *[J] Communications earth & environment, 2022, 3(1), 179.*

https://doi.org/10.1038/s43247-022-00504-8

摘要：位于北大西洋西部的缅因湾最近经历了快速的海洋暖化，但缺乏长期的仪器记录，阻碍了将这些重大水文变化纳入到气候背景当中。本文作者展示了多个 300 年跨度的地球化学记录（氧、氮以及之前发表的放射性碳同位素），这些记录都是在缅因湾西部的北极群岛贝壳上测量获得。通过结合气候模式的模拟和记录分析，表明缅因湾在过去 1000 年的大部分时间里经历了长期变冷，主要是由于火山强迫和北大西洋动力学所驱动。而这个降温趋势被 19 世纪后期开始的变暖所逆转，可能是由于大气温室气体浓度升高和北大西洋西部环流的变化。气候模式显示，上个世纪的变暖速度比该地区过去 1000 年的几乎任何一个 100 年周期都要快。

ABSTRACT: The Gulf of Maine, located in the western North Atlantic, has undergone recent, rapid ocean warming but the lack of long-term, instrumental records hampers the ability to put these significant hydrographic changes into context. Here we present multiple 300-year long geochemical records (oxygen, nitrogen, and previously published radiocarbon isotopes) measured in absolutely-dated Arctica islandica shells from the western Gulf of Maine. These records, in combination with climate model simulations, suggest that the Gulf of Maine underwent a long-term cooling over most of the last 1000 years, driven primarily by volcanic forcing and North Atlantic ocean dynamics. This cooling trend was reversed by warming beginning in the late 1800s, likely due to increased atmospheric greenhouse gas concentrations and changes in western North Atlantic circulation. The climate model simulations suggest that the warming over the last century was more rapid than

almost any other 100- year period in the last 1000 years in the region.

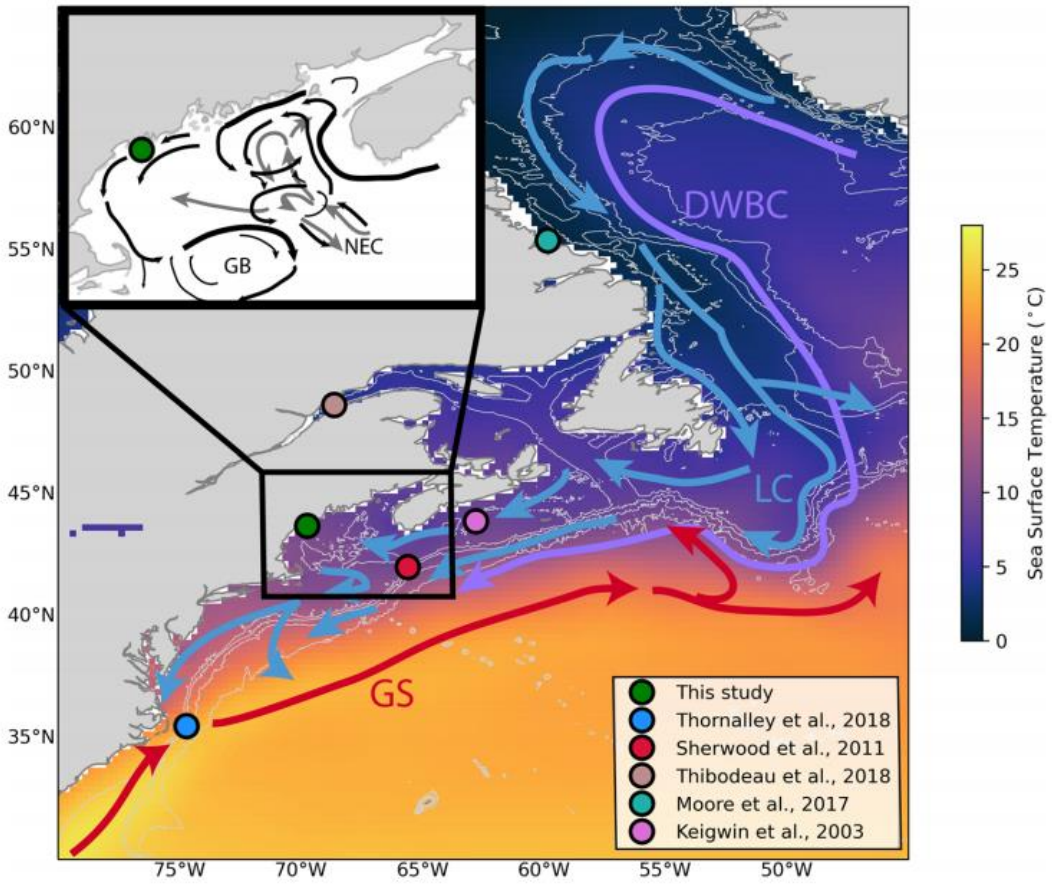

Figure 1. Map of study site and broader North Atlantic region. Arrows indicate schematic depictions of major ocean currents while colors indicate average sea surface temperatures. Markers indicate the location of the study site as well as other paleoceanographic records mentioned in the manuscript (see map legend). The site of the Boothbay Harbor sea surface temperature (SST) instrumental record is indistinguishable from the site of this study (green marker) on this map. Bathymetry contours are marked in white at 200, 1200, 2200, and 3200 m depths from Smith and Sandwell. SSTs are from the World Ocean Atlas 2018 climatological mean (from 1981 to 2010). The black box in the main figure shows the Gulf of Maine region highlighted in more detail in the inset. Black arrows in the inset depict surface currents, with gray arrows showing sub-surface currents. LC Labrador Current, DWBC Deep Western Boundary Current, GS Gulf Stream, NEC Northeast Channel, GB Georges Bank.

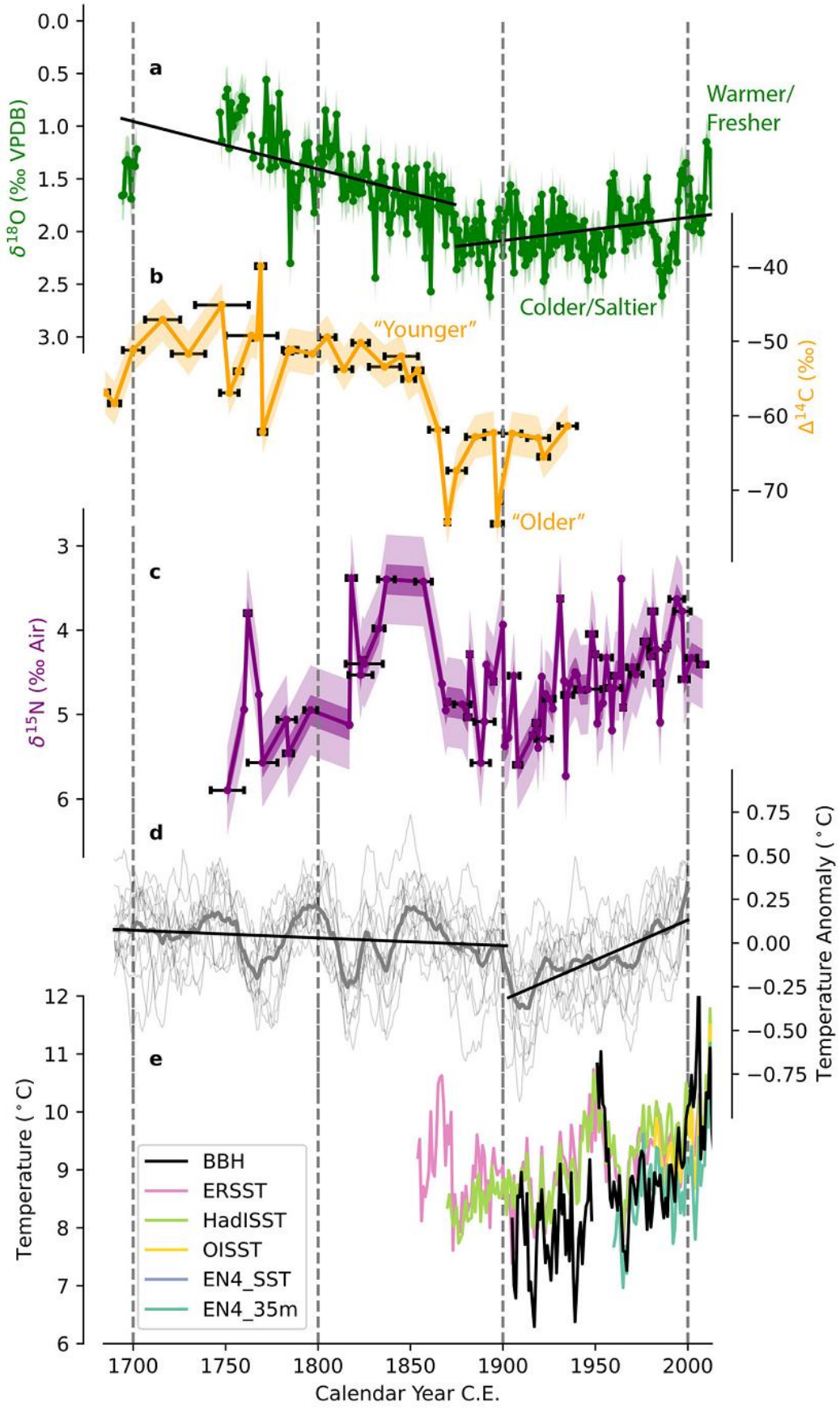
a
b
c
d
e
Warmer/
Fresher
Colder/Saltier
"Younger"
"Older"
δ^{18}O (‰ VPDB)
Δ^{14}C (‰)
δ^{15}N (‰ Air)
Temperature Anomaly (˚C)
Temperature (˚C)
Calendar Year C.E.
BBH
ERSST
HadISST
OISST
EN4_SST
EN4_35m

Figure 2. Geochemical, climate model, and instrumental time series. a Oxygen isotopes measured in Arctica island ice shells. Markers are the average value for that year. Black lines show the result of the segmented regression analysis. Light shading shows the average 1 σ of the data, calculated from those years when more than one shell was sampled, darker shading shows the average 1 σ analytical uncertainty. Note that the y-axis is inverted. b The age-corrected radiocarbon record, originally published in Lower‐Spies, et al.17. Horizontal error bars represent the amount of time incorporated in each sample. Shading shows the average 1 σ analytical uncertainty. c The nitrogen isotope record. Data after 1926 was previously published in Whitney, et al.26. Markers are the average value for that year. Horizontal bars represent the amount of time incorporated in each sample. Light shading shows the average 1 σ of the data, calculated for those years when more than one shell was sampled, darker shading shows the average 1 σ analytical uncertainty. Note that the y-axis is inverted. d The CESM-LME Gulf of Maine annual temperature anomaly time series, calculated at 35 m depth. Anomalies are calculated using the average of the entire record shown here. The bold line is the ensemble member mean, the thin lines show each of the 13 ensemble members with full transient forcing. The linear regression lines show the result of the segmented regression analysis on this record. e Temperature from instrumental records (BBH) and gridded data products (ERSST31, HadISST32, OISST34, EN436).

2. 近期月海活跃皱脊最新观测结果指示月球构造的时间与起源意义

翻译人：张琪 zhangq7@sustech.edu.cn

Nypaver C. A. & Thomson B. J., ***New observations of recently active wrinkle ridges in the lunar mare: Implications for the timing and origin of lunar tectonics*** *[J]. Geophysical Research Letters, 2022, e2022GL098975.*

https://doi.org/10.1029/2022GL098975

摘要：月球上构造特征的多样性表明月球岩石圈经历过复杂的变形历史。瓣状陡坡和皱脊便是两种由挤压应力形成的此类特征构造。叶状陡坡的脆状形态和横切关系，以及其与全球种群的相关性，被认为是能够证明它们形成的时间（<1.0 Ga）的证据，但对近期较活跃的皱脊的观测却并没有达到如此的规模。本文中，作者提出了针对 1116 个近期较活跃的（~0.056-1.5 Ga）月海皱脊的最新观测情况。观测结果表明，最近较活跃的皱脊近 90%分布在海缘盆地。此外，作者发现皱脊的方向与轨道衰退和全球收缩以及与 South Pole-Aitken 盆地相关的一组处于持续激活状态的残余结构所产生的预测应力场之间存在空间的相关性。

ABSTRACT: The variety of tectonic features on the Moon indicates that the lunar lithosphere has undergone a complex deformational history. Lobate scarps and wrinkle ridges are two such tectonic features that have resulted from compressional stresses. The crisp morphologies and cross cutting relations associated with a global population of lobate scarps have been cited as evidence for their recent (<1.0 Ga) formation, but observations of recently active wrinkle ridges have not been made on a similar scale. Here, we present new observations of 1,116 recently active (~0.056-1.5 Ga) wrinkle ridge segments on the lunar maria. Our results indicate that clusters of recently active wrinkle ridges are distributed across ~90% of nearside mare basins. Spatial correlations were noted between wrinkle ridge orientations with predicted stress fields from both orbital recession and global contraction as well as ongoing reactivation of a residual set of structures associated with the South

Pole–Aitken basin.

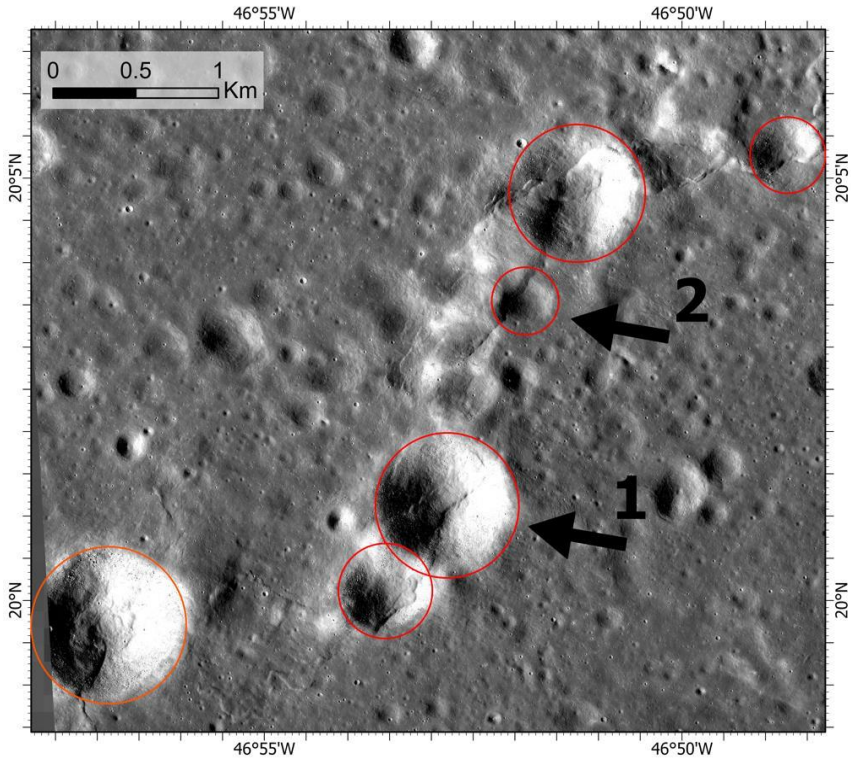

Figure 1. LROC NAC image showing: 1) a degraded crater crosscut by both parallel wrinkle ridge scarps and 2) crater deformation by a single wrinkle ridge scarp (LROC NAC M1219258635RE). Red circles represent tectonically deformed impact crater rims.

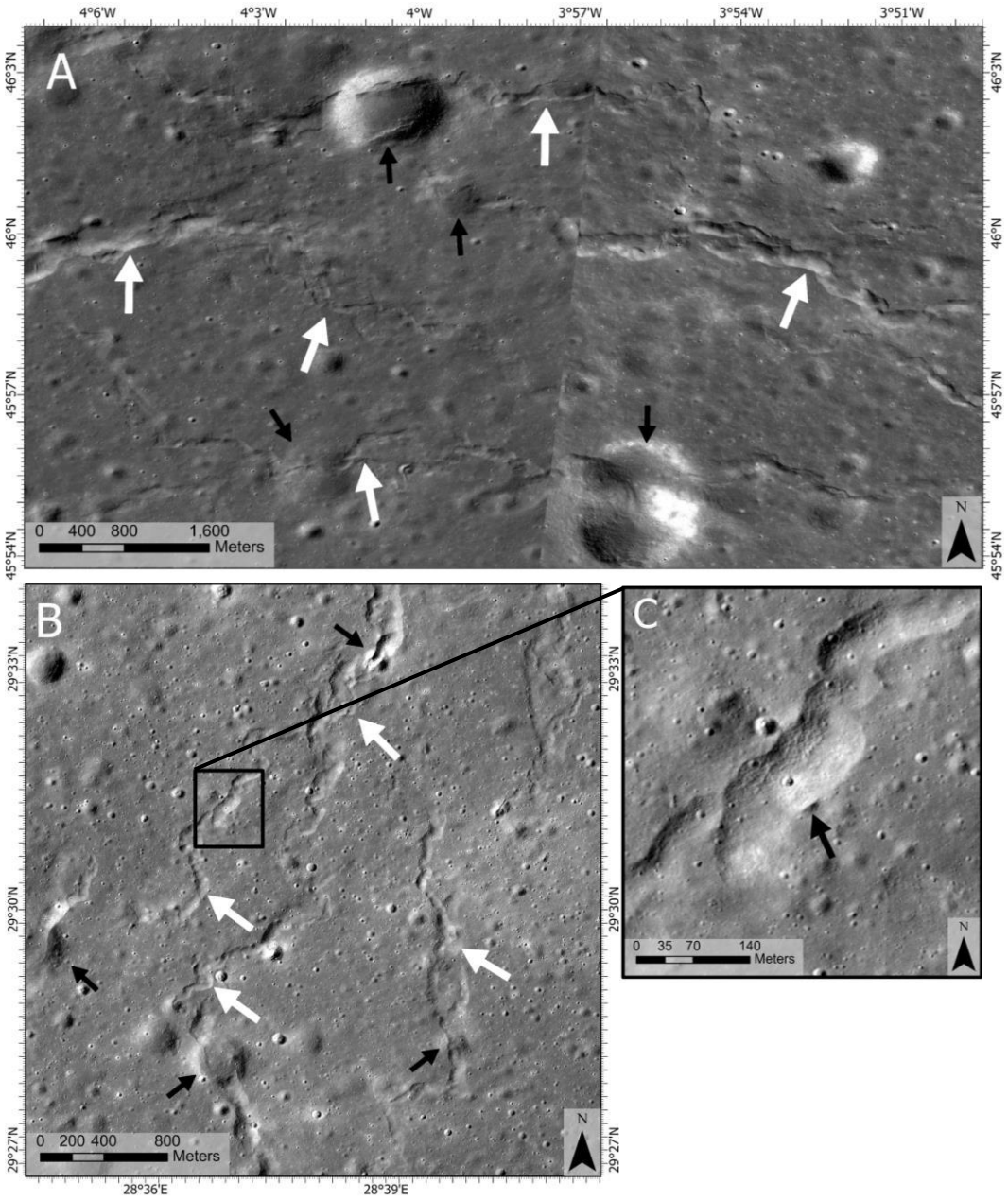

Figure 2. Examples of recently active wrinkle ridge systems located in N. Mare Imbrium (a) (LROC NAC M1274280167RE, M1236649139LE) and E. Mare Serenitatis (b) (LROC NAC M1289319410LE). (c) Image subset depicting a ~35 m-diameter impact crater crosscut by a recently active wrinkle ridge. White arrows indicate recently active ridges and black arrows show crosscut craters in all images.

3. 欧洲西北部白垩纪末大灭绝期团簇同位素记录的气候趋势

翻译人：张靖宇 zhangjy6@sustech.edu.cn

O'Hora H E, Petersen S V, Vellekoop J, et al. ***Clumped-isotope-derived climate trends leading up to the end-Cretaceous mass extinction in northwest Europe****[J]. Climate of the Past, 2021: 1-28*

https://doi.org/10.5194/cp-18-1963-2022

摘要：白垩纪末期的古温度重建记录了当地和全球的气候趋势，其中一些是由 Deccan Traps 火山活动的温室气体排放和相关的反馈作用所驱动的。在此，我们提出了一个新的基于团簇同位素的古温度记录，该记录来自荷兰东南部和比利时东北部 Maastrichtian 典型地区的双壳动物化石。团簇同位素数据记录的平均温度为 20.4±3.8°C，与其他 Maastrichtian 的温度估计一致，该地区在晚白垩纪（67.1-66.0 Ma）的平均海水 $\delta^{18}O$ 值为 0.2±0.8‰VSMOW。在 66.4 Ma 的显著温度上升被解释为全球定义的晚 Maastrichtian 变暖事件的区域表现，将 Deccan Traps 的二氧化碳排放与 Maastricht 地区的气候变化联系起来。与温度变化相吻合的海水 $\delta^{18}O$ 值的波动表明，来自南方的温暖咸水和来自北冰洋的较冷较新鲜的水交替影响。新的古温度记录有助于了解区域和全球气候对大规模火山活动和海洋环流变化的反应，导致灾难性的大灭绝。

ABSTRACT: Paleotemperature reconstructions of the end Cretaceous interval document local and global climate trends, some driven by greenhouse gas emissions from Deccan Traps volcanism and associated feedbacks. Here, we present a new clumped-isotope-based paleotemperature record derived from fossil bivalves from the Maastrichtian type region in southeastern Netherlands and northeastern Belgium. Clumped isotope data document a mean temperature of 20.4 ± 3.8 °C, consistent with other Maastrichtian temperature estimates, and an average seawater $\delta^{18}O$ value of 0.2±0.8‰ VSMOW for the region during the latest Cretaceous (67.1-66.0 Ma). A notable temperature increase at ~ 66.4 Ma is interpreted to be a regional manifestation of the globally defined Late Maastrichtian Warming Event, linking Deccan Traps volcanic CO_2 emissions to climate change in the Maastricht region. Fluctuating seawater $\delta^{18}O$ values coinciding with

temperature changes suggest alternating influences of warm, salty southern-sourced waters and cooler, fresher northern-sourced waters from the Arctic Ocean. This new paleotemperature record contributes to the understanding of regional and global climate response to large-scale volcanism and ocean circulation changes leading up to a catastrophic mass extinction.

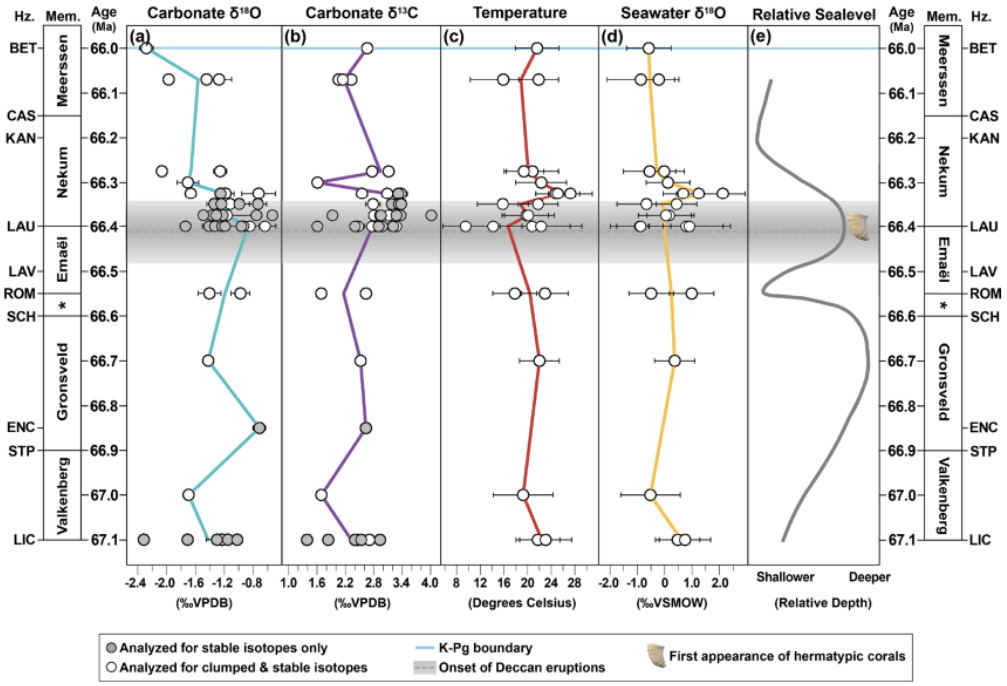

Figure 1. Isotopic compositions and paleotemperatures of fossil shells compared to inferred relative sea level in the Maastricht Formation. Error bars represent 1 SD for $\delta^{18}O$ (a) and $\delta^{13}C$ (b) and represent external 1 SE for temperature (c) and $\delta^{18}Osw$ (d) (see Sect. 3.3). All samples failing diagenetic screening criteria have been removed. Colored lines pass through horizon means. Age model from Vellekoop et al. (2022; Table S3). The relative sea level curve (e) is based on Schiøler et al. (1997), adjusted to the age model used in this study. Hermatypic coral appearance data (e) are from Leloux (1999). Onset of the main Deccan Traps eruptions (grey dotted line) at 66.413±0.067 Ma (Sprain et al., 2019).

4. 逆冲作用导致的河流重组解释长江第一湾形成于晚渐新世-早中新世

翻译人：刘伟 inewway@163.com

Zhang D, Cao K, Yuan X. Late Oligocene-early Miocene Origin of the First Bend of the Yangtze River explained by thrusting-induced river reorganization [J]. Geomorphology, 2022: 108303.

https://doi.org/10.1016/j.geomorph.2022.108303

摘要：长江第一湾的起源是理解近代长江诞生的关键。尽管有相当多的研究工作，第一湾形成的时间和机制仍然存在极大争议。通过对金沙江三条支流的河流剖面反演，结合区域构造和地貌解释，得出了第一湾的形成时间在 28-20 Ma。西藏东南部玉龙逆冲断带的活动与河流初始下切的时空一致性表明，逆冲作用是第一湾河网重塑的根本原因。这些结果重新解释了第一湾以南剑川盆地沉积环境由辫状河到沼泽状湖泊的变化，记录了~36 ~ 35 Ma 向南流的古金沙河和水罗河被岩浆作用破坏的过程。渐新世晚期至中新世早期，由于玉龙逆冲断裂带的逆冲作用，岩石抬升，导致古水洛河北移，剑川盆地被剥露。古水洛河的改道可以用玉龙逆冲断裂带下盘下游河流的袭夺来解释。随后，逆冲作用引起的局部基准面下降导致了快速的溯源侵蚀，上游的年龄越来越年轻，导致了第一湾的形成。第一湾于 28～20 Ma 形成的新年龄和上游更年轻的年龄组合表明，金沙江以 62±18 mm/年的速度向北扩张。综合来看，本文的结果表明，第一湾的形成可能是 28～20 Ma 的逆冲作用导致的，之后长江形成。

ABSTRACT: The origin of the First Bend of the Yangtze River is key to understanding the birth of the modern Yangtze River. Despite considerable efforts, the timing and mechanism of formation of the First Bend remain highly debated. Inverse river-profile modeling of three tributaries (Chongjiang, Lima, and Gudu) of the Jinsha River, integrated with regional tectonic and geomorphic interpretations, allows the onset of incision at the First Bend to be constrained to 28–20 Ma. The spatio-temporal coincidence of initial river incision and activity of Yulong Thrust Belt in southeastern Tibet highlights thrusting to be fundamental in reshaping the pre-existing stream network at the First Bend. These results enable us to reinterpret a change in sedimentary environment from a braided river to a swamp-like lake in the Jianchuan Basin south of the First Bend, recording the destruction of the hypothesized southwards-flowing paleo-Jinsha and Shuiluo Rivers at ~36–35 Ma by magmatism. During the late Oligocene-early Miocene, the paleo-Shuiluo

River was diverted to the north by focused rock uplift due to thrusting along the Yulong Thrust Belt, which also led to exhumation of the Jianchuan Basin. Diversion of the paleo-Shuiluo River can be explained by capture from a downstream river in the footwall of the Yulong Thrust Belt. Subsequent rapid headward erosion, that was caused by thrusting-induced drop of local base level, is recorded by upstream younging ages for the onset of incision and led to the formation of the First Bend. The combination of new ages for the onset of incision at 28–20 Ma at the First Bend and younger ages upstream indicates northwards expansion of the Jinsha River at a rate of 62 ± 18 mm/yr. Our results suggest that the origin of the First Bend was likely triggered by thrusting at 28–20 Ma, after which the Yangtze River formed.

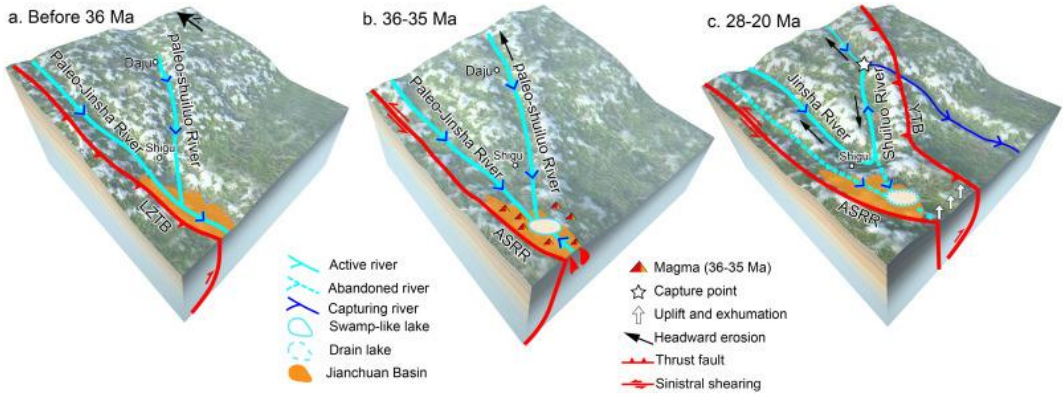

Figure 1. Model for the origin of the First Bend of the Yangtze River. (a) Before 36 Ma, the southward-flowing paleo-Jinsha River and paleo-Shuiluo River merged in the Jinchuan Basin (modified from Clark et al., 2004, Clift et al., 2020, and Feng et al., 2021); (b) At 36–35 Ma, the former southward-flowing paleo-Jinsha River and its tributary (paleo-Shuiluo River) were disrupted by magmatism and a swamp-like endorheic lake formed; (c) At 28–20 Ma, the paleo-Jinsha River was abandoned and the paleo-Shuiluo River was diverted to the north by uplift of the Jianchuan Basin due to thrusting along the YTB, forming the First Bend. A river in the footwall of the YTB captured the paleo-Shuiluo River, which led to headward incision.

5. 末次冰消期地中海中部的降雨随北半球高纬温度变化而变化

翻译人：杨会会 11849590@mail.sustech.edu.cn

Columbu A, Spotl C, Fohlmeister J, et al., ***Central Mediterranean rainfall varied with high northern latitude temperatures during the last deglaciation [J].*** *Communications Earth & Environment, 2022, 3, 181.*

https://doi.org/10.1038/s43247-022-00509-3

摘要：与当前气候变化的影响类似，末次冰消期（Termination I，冰期终止期 I）迅速改变了北半球的纬度温度和冰盖范围，以及大西洋经向翻转环流。然而，目前还不清楚这些变化是如何传播和影响地中海中部大陆降雨变率的。这妨碍了对未来全球变暖将如何影响地中海地区的全面了解。在这里，我们基于意大利南部一根新的石笋 $\delta^{18}O$ 序列，重建了地中海中部跨越冰期终止期 I 时期的高分辨率降雨变化。在冰期终止期 I，大西洋水汽的可获得性随北纬温度的升高（降低）和冰盖的降低（增加）而变化，促进了大西洋经向翻转环流强度的增加（降低），并导致地中海气候相对湿润（干燥）。考虑到未来气候变暖的趋势，本研究强调了高纬度气候变化对人口密集的地中海地区降雨变化的影响。

ABSTRACT: Similarly to the effects of current climate change, the last deglaciation (Termination I) rapidly altered northern latitude temperatures and ice-sheet extent, as well as the Atlantic Meridional Overturning Circulation. However, it is still unclear how these changes propagated and impacted the central Mediterranean continental rainfall variability. This prevents a full understanding on how global warming will affect Mediterranean areas in the future. Here, we present a high-resolution reconstruction of rainfall changes in the central Mediterranean across Termination I, based on a novel $\delta^{18}O$ time series from a southern Italian stalagmite. Across Termination I the availability of Atlantic moisture varied in response to northern latitude temperature increases (decreases) and ice-sheet decreases (increases), promoting a higher (lower) intensity of the Atlantic Meridional Overturning Circulation, and resulting in a relatively wetter (drier) climate in the Mediterranean. In the light of future warming, this study emphasizes the role

of high-latitude climate changes in causing rainfall variation in highly populated Mediterranean areas.

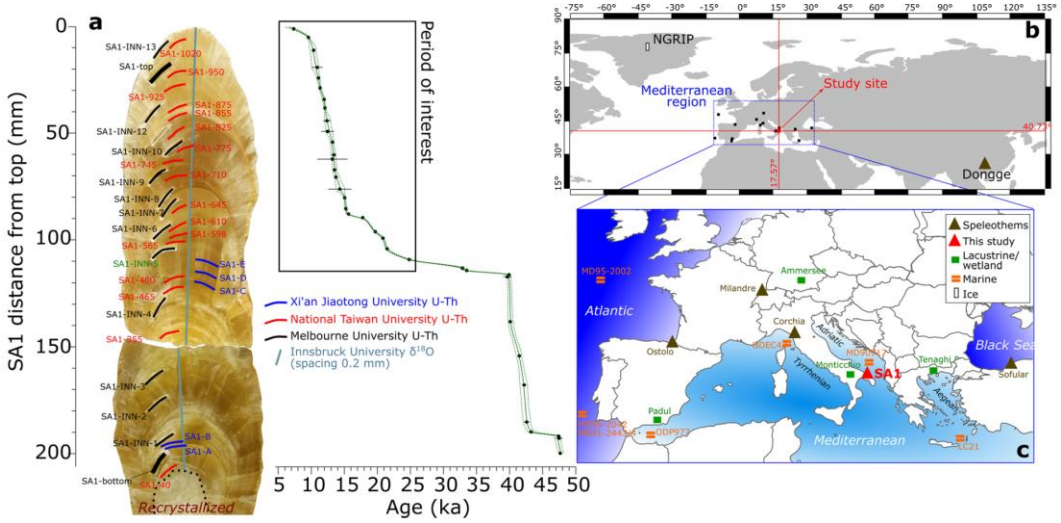

Figure 1. Sample, analyses and study site. a SA1 stalagmite and analyses accomplished in this study. Colored bars refer to U-Th dating at Xi'an Jiaotong (blue), National Taiwan (red) and Melbourne (black) Universities, while the blue line marks $\delta^{18}O$ analyses (methods) carried out at Innsbruck University. The age model is reported with dots and 2σ error bars (indicating the U-Th ages) and their relative interpolation (green line = average model; dotted lines = propagation of ±2σ uncertainties). b, c Study site and other records discussed in the text.

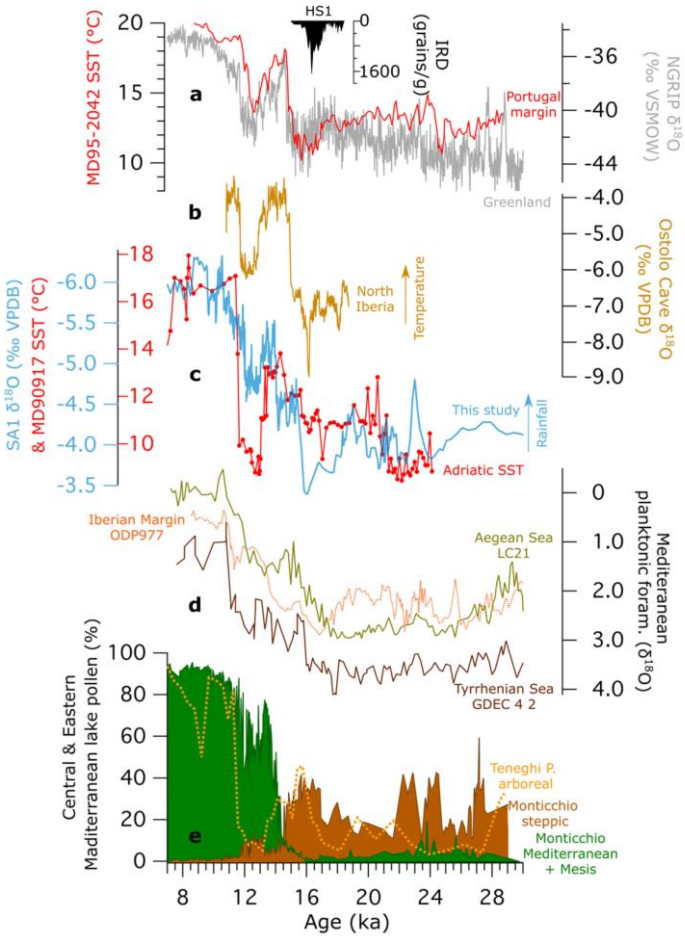

Figure 2. a Ice rafted debris (IRD) from the Gulf of Biscay related to the HS1 event (black fill), Portugal Margin SST (red line) and Greenland ice-core $\delta^{18}O$ (grey line). b Ostolo Cave stalagmite $\delta^{18}O$, a proxy for northern Iberian temperature (yellow line). c SA1 $\delta^{18}O$ (light blue line, this study) taken as palaeo-rainfall proxy and Adriatic SST (red line). d Planktonic foraminifera from the Aegean Sea (brown line, the Tyrrhenian Sea (purple line48) and the Iberian Margin (dotted orange line), proxies for Mediterranean planktonic-derived temperatures. e Pollen from Monticchio (green and brown fill) and Tenaghi Philippon lakes (yellow dotted line), representing vegetation changes. For locations see Fig. 1.

6. 南岭西部大坪沼泽湖相沉积物正构烷烃记录追踪的有机质来源及其对末次冰期以来气候变化的响应

翻译人：王浩森 11930841@mail.sustech.edu.cn

Lin Durui, Zhong Wei, Lin Yingbing, et al. ***Organic matter source traced by n-alkane records derived from lacustrine sediments from Daping swamp in the western Nanling Mountains (South China) and its response to climatic variability since the last Deglacial*** *[J]. Palaeogeography, Palaeoclimatology, Palaeoecology, 2022: 111217.*

https://doi.org/10.1016/j.palaeo.2022.111217

摘要：先前的记录揭示了中国南方南岭西部大坪沼泽湖沉积物中保存完好且规模较长的地质信息。然而，沉积物中有机质（OM）的确切来源及其对气候变化的响应仍不清楚。在本研究中，我们提出了从该沼泽的湖泊沉积物中提取的 15.3 kyr 正烷烃记录，以探索 OM 来源以及 OM 输入与气候变化之间的关系。结果表明，沉积物中正构烷烃组成以长链烷烃（C_{27}-C_{31}）为主，表明有机质主要来源于陆生高等植物和水生植物。正构烷烃数据进一步证实，OM 源的变化与气候变化控制的表面侵蚀-迁移-沉积过程有关。湖泊水位变化也受气候条件的调节，在影响有机质积累方面发挥了重要作用；温暖和潮湿的条件将导致湖泊水位上升，有利于更多的水生有机质和更少的陆地有机质输入，反之亦然。亚洲夏季风强度的变化受低纬度过程（如太阳辐射、热带辐合带和厄尔尼诺/南方涛动）以及高纬度过程（例如北大西洋融水输入）的动态变化的调节，与沉积物中的 OM 积累密切相关。

ABSTRACT: Previous multi-proxy records have revealed the advantages of well-preserved and long-scale geological archives from the lake sediments of Daping swamp in the western Nanling Mountains in South China. However, the exact organic matter (OM) sources in the sediments and their response to climatic variability still remain unclear. In this study, we present a 15.3-kyr *n*-alkane record extracted from lacustrine sediments in this swamp to explore the OM sources and the relationship between OM input and climatic changes. The results indicated that the *n*-alkane composition in sediments was dominated by long-chain *n*-alkanes (C_{27}-C_{31}), implying that the OM

mainly originated from the terrestrial higher plants and emergent aquatic plants. The *n*-alkane data further verified that changes in OM sources were related to the surface erosion-transportation-deposition processes controlled by climatic changes. Lake level change, which was also regulated by climate conditions, played an important role in impacting OM accumulation; warmer and wetter conditions would result in rising lake levels that favored more aquatic OM and less terrestrial OM input, and vice versa. Variability of the Asian summer monsoon intensity regulated by the dynamic variations in low-latitude processes (e.g., solar insolation, intertropical convergence zone, and El Niño/Southern Oscillation), as well as high-latitude processes (e.g., meltwater input in the North Atlantic), was closely related to the OM accumulation in sediments.

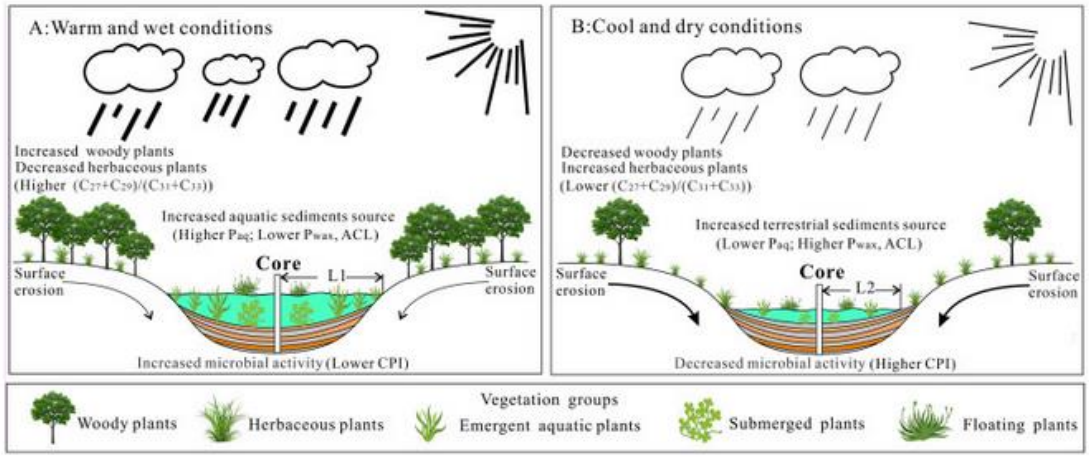

Figure 1. Schematic model indicating the OM accumulation patterns revealed by *n*-alkane proxies in the sediments under different climatic conditions in Daping swamp. (A): under warm and wet conditions; (B): under cool and dry conditions.

7. 从观测和模拟评价地幔控制地球发电机的指标

翻译人：李海 12031330@mail.sustech.edu.cn

Korte M, Constable C, Panovska S J, et al. ***Indicators of mantle control on the geodynamo from observations and simulations*** *[J]. Frontiers in Earth Science, 2022, 1472.*

https://doi.org/10.3389/feart.2022.957815

摘要：核幔边界热流横向变化的影响是否可以在古地磁记录中检测到，一直存在争议。它们的特征通常在虚地磁极（VGP）路径记录中寻找，这些路径在极性转换和漂移期间表现出特定的经向特征。这些特征通常与下地慢大型低地震速度区（LLVPs）的热效应有关，但由于分辨率较低而遭受质疑。近年来的古地磁模型涵盖了 1-100 ka 的不同阶段，其中三个包含了地磁漂移，使我们可以用最小磁场强度分布补充对 VGP 路径空间分布的评估。采用四个不同的数值发电机模拟的模型评估结果的可靠性，有无可变热边界条件，包括稳定的地磁极性、漂移和倒转。结果表明，VGP 分布在将热 CMB 结构的影响与实际古地磁观测的地理变化联系起来不如最小磁场强度有用，因为 VGP 相关性强烈依赖于足够数量的相对罕见事件的高空间分辨率。这些结果为评估四个古磁场模型的对比观测提供了基础。基于现有数据的时空分辨率，VGP 位置的分布提供了不可靠的结果。尽管东半球的结果很复杂，但全球最小磁场分布与 LLVPs 以外区域的粗略相关性给出了一些地幔控制的迹象，这可能突出了下地慢热和成分变化之间的半球平衡的不确定性。然而，获得其他地磁场特征（如 CMB 的强度和经向场）为使用扩展和改进的全球地磁场模型从观测方面解决地幔对地球发电机的影响问题提供了有力的证据。

ABSTRACT: There has been longstanding controversy about whether the influence of lateral variations in core-mantle boundary heat flow can be detected in paleomagnetic records of geomagnetic field behavior. Their signature is commonly sought in globally distributed records of virtual geomagnetic pole (VGP) paths that have been claimed to exhibit specific longitudinal preferences during polarity transitions and excursions. These preferences have often been linked to

thermal effects from large low seismic velocity areas (LLVPs) in the lowermost mantle, but the results have been contested because of potential sensitivity to sparse temporal and spatial sampling. Recently developed time varying global paleofield models spanning various time intervals in 1–100 ka, three of which include excursions, allow us to complement assessments of spatial distributions of transitional VGP paths with distributions of minimum field intensity. Robustness of the results is evaluated using similar products from four distinct numerical dynamo simulations with and without variable thermal boundary conditions and including stable geomagnetic polarity, excursions and reversals. We determine that VGP distributions are less useful than minimum field intensity in linking the influences of thermal CMB structure to geographical variations in actual paleofield observables, because VGP correlations depend strongly on good spatial sampling of a sufficient number of relatively rare events. These results provide a basis for evaluating comparable observations from four paleofield models. The distribution of VGP locations provide unreliable results given the restricted time span and available data locations. Rough correlations of global distributions of minimum intensity with areas outside the LLVPs give some indications of mantle control during excursions, although the results for the eastern hemisphere are complex, perhaps highlighting uncertainties about the hemispheric balance between thermal and compositional variations in the lowermost mantle. However, access to other geomagnetic properties (such as intensity and radial field at the CMB) provides a strong argument for using extended and improved global paleofield models to resolve the question of mantle influence on the geodynamo from the observational side.

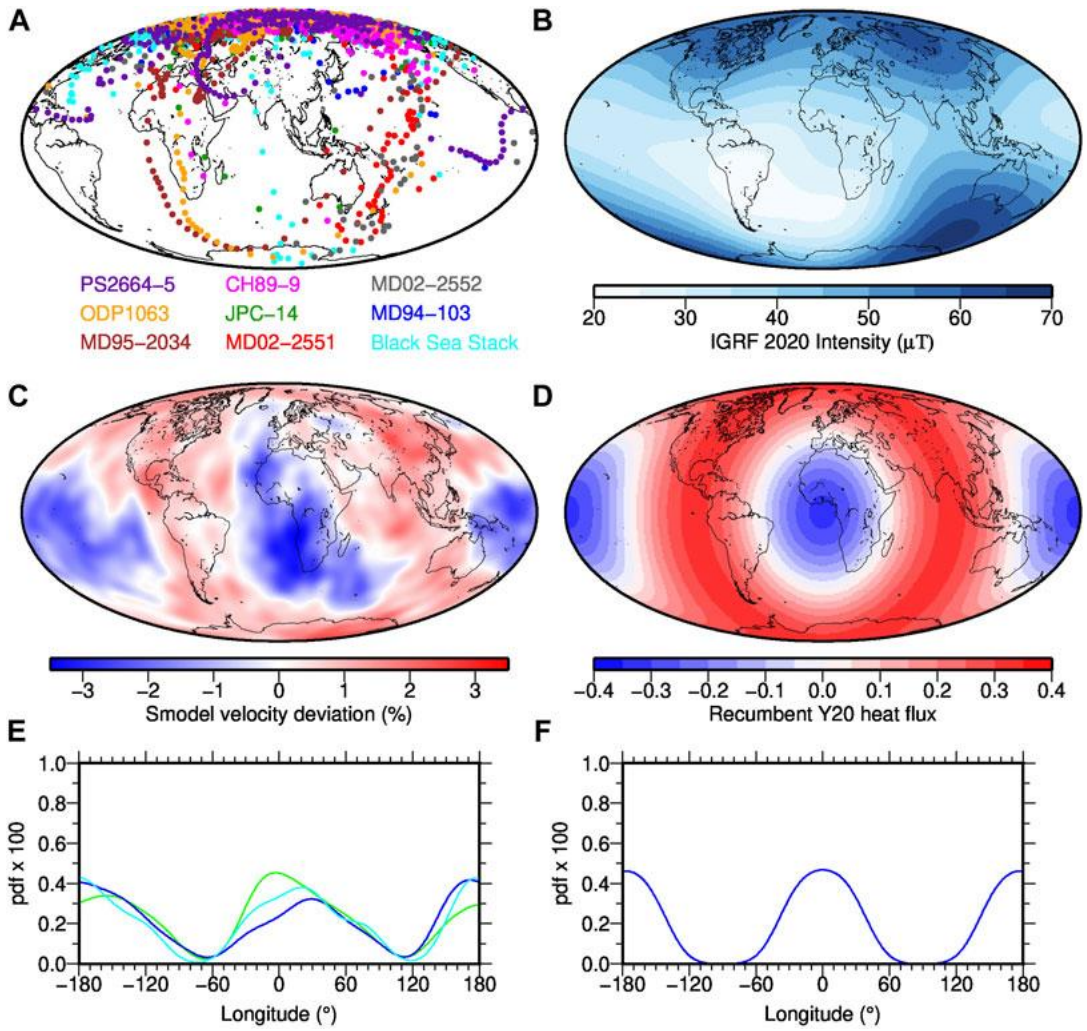

Figure 1. (A) Reproduction of VGP paths for the Laschamp excursional paleomagnetic data compiled by Laj and Channell (2015), augmented with the Black Sea record of Nowaczyk et al. (2012). Note that because of ambiguity in setting the average declination PS2664-5 is shifted in longitude relative to the original plot; note further that the central longitude is different in panel (A) than in panels (B-F). (B) Geomagnetic field strength for 2020CE based on IGRF (Alken et al., 2021); (C) Seismic shear wave velocity perturbation at the CMB from model Smodel with blue areas representing LLVPs (see Section 2); (D) Heat flux pattern corresponding to recumbent Y02 used for the inhomogeneous CMB condition in the NDS (with continents shown only for ease of comparison). (E) Latitudinally averaged probability density of LLVP areas from seismic model Smodel (green) and below average heat flux regions from models Tlin (blue) and Tp3 (cyan) (see Section 2) as a function of longitude, and (F) the same for below average heat flow from the recumbent Y02 pattern (blue).

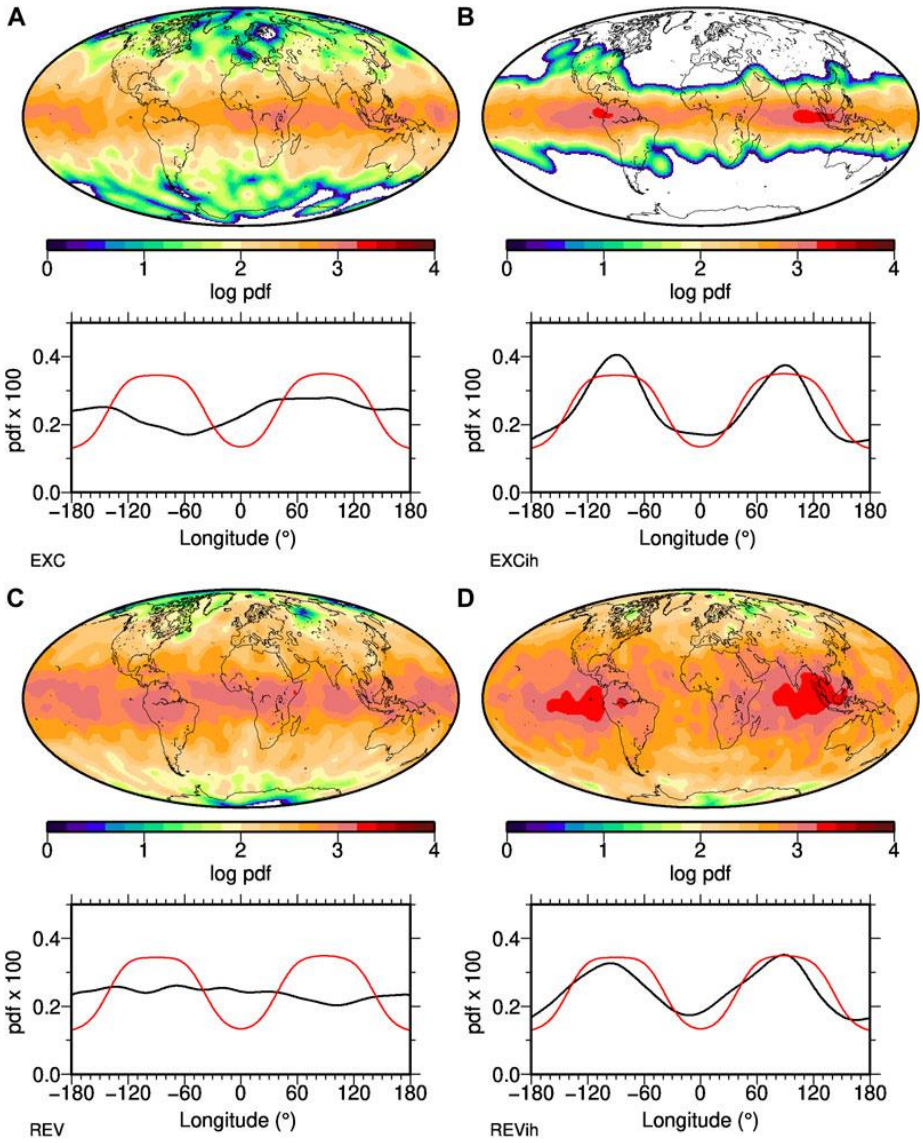

Figure 2. Distributions of intensity minima in four different numerical dynamo simulations, with continents shown for ease of comparison to PFM results. The top panels give their global density distribution, the bottom panels the longitudinal density distribution (black line) in comparison to the distribution of above average CMB heat flux or "non-LLVP" areas (red) from a recumbent Y02 structure. Simulations EXC (A) and REV (C) have homogeneous heat flow, while EXCih (B) and REVih (D) have the recumbent Y02 heat flow imposed. EXC (A) and EXCih (B) are more strongly dipole-dominated than REV (C) and REVih (D). Global minima never occur in the white areas in panel b, due to the strong dipole dominance of that simulation.

8. 高纬地区过去 22 kyr 虚地磁极（VGP）路径重建：径向磁通量斑块对 VGP 的吸引作用

翻译人：张伟杰 12031188@mail.sustech.edu.cn

Caricchi C, Campuzano S A, Sagnotti L, et al. ***Reconstruction of the Virtual Geomagnetic Pole (VGP) path at high latitude for the last 22 kyr: The role of radial field flux patches as VGP attractor****[J]. Earth and Planetary Science Letters, 2022, 595: 117762.*

https://doi.org/10.1016/j.epsl.2022.117762

摘要：地磁场变化重建在地球发电机建模和地核动力学的认识方面具有重要意义。最近基于地磁测量的工作显示，在过去的二十年中，北极的位置在很大程度上是由加拿大和西伯利亚下两个相互竞争的磁通量瓣的影响决定的。为了解过去磁通量瓣的起伏是否影响了地磁古极的路径，我们从 Barents 海西北缘和 Spitsbergen（北极）西缘岩芯获得了过去 22 kyr 更新的年代学和地磁场长期变化的新记录。重建了该段时间内虚拟地磁极的路径，并与从最新模型获得的核幔边界处地磁场的径向分量图进行了比较。该 VGP 路径包括其位置稳定的几个世纪和其运动加速的几个世纪。我们识别出顺时针和逆时针的 VGP 路径，其主要在北极地区内核切线圆柱的表面投影内形成。VGP 的路径似乎紧随正的径向场磁通量斑块，尤其是位于西伯利亚和加拿大地区的磁通量斑块，但也包括例如引起 Levantine 铁器时代磁异常的那些可能导致特殊的古地磁场特征的磁通量斑块。

ABSTRACT: Reconstruction of geomagnetic field changes has a strong potential to complement geodynamo modeling and improve the understanding of Earth's core dynamics. Recent works based on geomagnetic measurements pointed out that over the last two decades the position of the north magnetic pole has been largely determined by the influence of two competing flux lobes under Canada and Siberia. In order to understand if the waxing and waning of magnetic flux lobes have driven the path of geomagnetic paleopoles in the past, we present an augmented and updated record of the chronology and paleosecular variation of geomagnetic field for the last 22 kyr derived from

sedimentary cores collected along the north-western margin of Barents Sea and western margin of Spitsbergen (Arctic). The path of the virtual geomagnetic pole (VGP) has been reconstructed over this time period and compared with the maps of the radial component of the geomagnetic field at the core-mantle boundary, obtained from the most recent models. The VGP path includes centuries during which the VGP position is stable and centuries during which its motion accelerates. We recognize both clockwise and counterclockwise VGP paths, mostly developing inside the surface projection of the inner core tangent cylinder in the Arctic region. The VGP path seems to follow the appearance of Br patches of normal magnetic flux, especially those located under Siberia and Canada areas, but also those that may cause peculiar paleomagnetic features such as the Levantine Iron Age Anomaly.

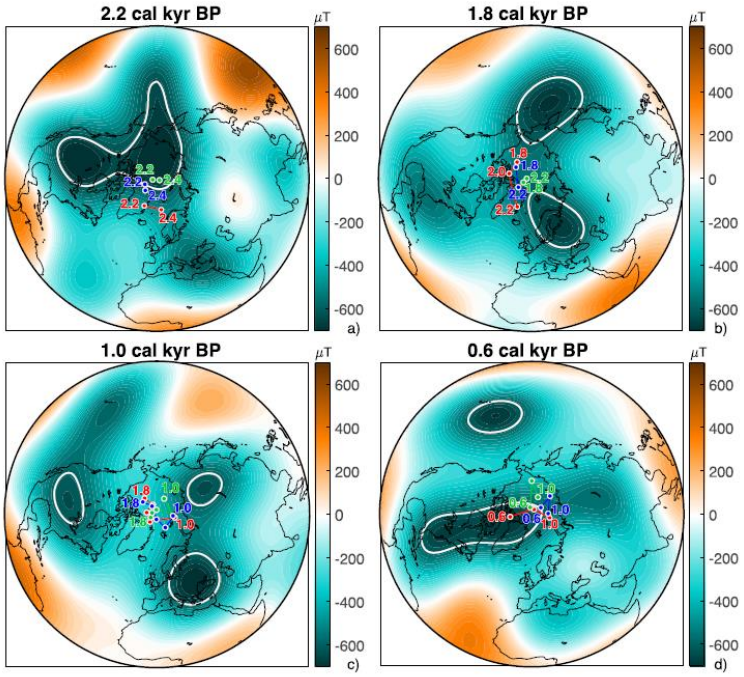

Figure 1. VGP path reconstruction of NBS22.2k PSV stack (in red), Levant (in blue) and Mexico (in green), overlaid on maps of the radial component of the geomagnetic field (in μT) at the Core-Mantle Boundary from SHAWQ-Iron Age model in (a) 2.2 cal kyr BP_{2000} and SHAWQ2k in (b) 1.8 cal kyr BP_{2000} (c) 1.0 kyr BP_{2000} (d) 0.6 cal kyr BP_{2000}. Present refers to 2000 CE. White contour lines correspond to −625 μT for (a) and −580 μT for (b-d) and highlight the NFPs that act as VGP attractor according to our interpretation.

9. 新生代暖期氧化作用的增强

翻译人：张亚南 zhangyn3@mail.sustech.edu.cn

Auderset A, Moretti S, Taphorn B, et al. ***Enhanced ocean oxygenation during Cenozoic warm periods*** *[J]. Nature, 2022, 609, 77-82.*

https://doi.org/10.1029/2022GL097967

摘要：溶解氧（O_2）对大多数海洋生态系统至关重要，推动生物有机质的呼吸作用以及促进碳和营养物质的循环。氧含量测量结果表明，在全球变暖的情况下海洋缺氧区（ODZs）正在扩张。然而，模拟无法提供未来短期以及长期 ODZ 变化的清晰画面。古气候记录可以提供比现今更温暖时期 ODZ 可能的变化范围。文中，作者通过有孔虫中的氮同位素发现，在中中新世气候最适期（MMCO）和早始新世气候最适期（EECO），东赤道太平洋的水体反硝化作用显著减弱。由于反硝化作用仅限于缺氧水域，因此文中的结果表明，在这两个新生代持续温暖期，ODZ 是收缩的，而非扩张。ODZ 的收缩可能是由于热带太平洋上升流引起的生物生产力下降，这将减少次表层对氧气的消耗。另外，南大洋深部通风系统的活跃可能削弱了生物碳泵，从而增加了深海的氧气。这一机制决定了 ODZ 的收缩是与全球变暖同步发生，还是需要几百年或千年时间形成。因此，虽然从新生代得出的结论并不一定适用于近期的预测，但它们可能意味着全球变暖最终可能导致 ODZ 收缩。

ABSTRACT: Dissolved oxygen (O_2) is essential for most ocean ecosystems, fuelling organisms' respiration and facilitating the cycling of carbon and nutrients. Oxygen measurements have been interpreted to indicate that the ocean's oxygen-deficient zones (ODZs) are expanding under global warming. However, models provide an unclear picture of future ODZ change in both the near term and the long term. The paleoclimate record can help explore the possible range of ODZ changes in warmer-than-modern periods. Here we use foraminifera-bound nitrogen (N) isotopes to show that water-column denitrification in the eastern tropical North Pacific was greatly reduced during the Middle Miocene Climatic Optimum (MMCO) and the Early Eocene Climatic Optimum (EECO).

Because denitrification is restricted to oxygen-poor waters, our results indicate that, in these two Cenozoic periods of sustained warmth, ODZs were contracted, not expanded. ODZ contraction may have arisen from a decrease in upwelling-fuelled biological productivity in the tropical Pacific, which would have reduced oxygen demand in the subsurface. Alternatively, invigoration of deep-water ventilation by the Southern Ocean may have weakened the ocean's 'biological carbon pump', which would have increased deep-ocean oxygen. The mechanism at play would have determined whether the ODZ contractions occurred in step with the warming or took centuries or millennia to develop. Thus, although our results from the Cenozoic do not necessarily apply to the near-term future, they might imply that global warming may eventually cause ODZ contraction.

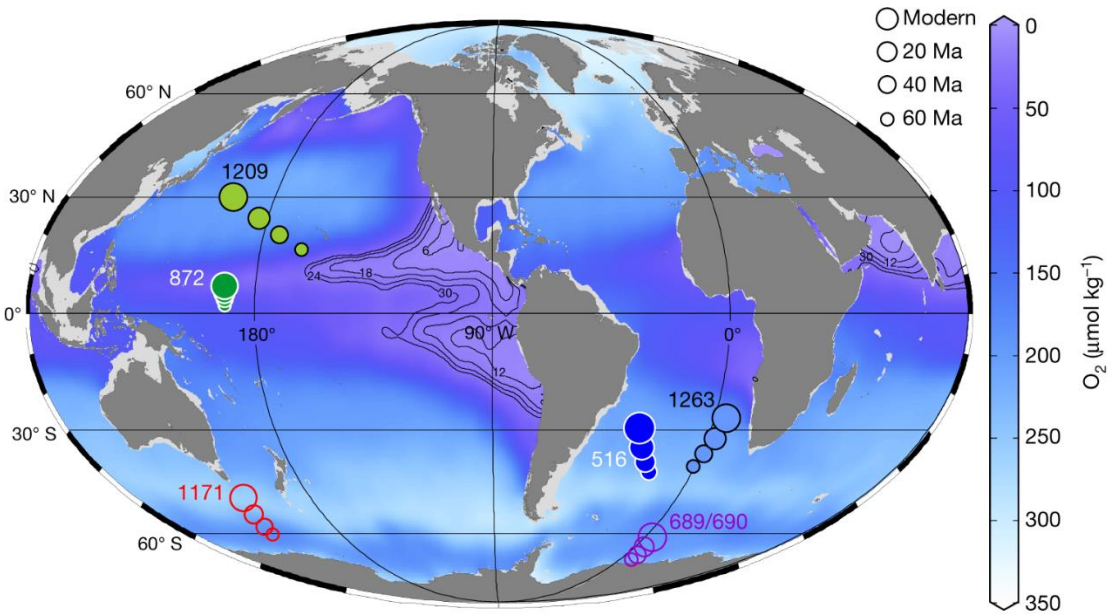

Figure 1. Sites from which core data are reported or discussed, plotted over modern dissolved O_2 concentrations at 350 m water depth. Tectonically driven changes in site locations are shown with symbol size (see legend). Filled circles indicate cores with FB-$\delta^{15}N$ data, from this study (872/516) and from Kast et al. (1209/1263), and open circles indicate cores with foraminiferal $\delta^{18}O$ data discussed in the text (and references therein). Dissolved O_2 concentrations (in µmol kg^{-1}) are shown in colour.

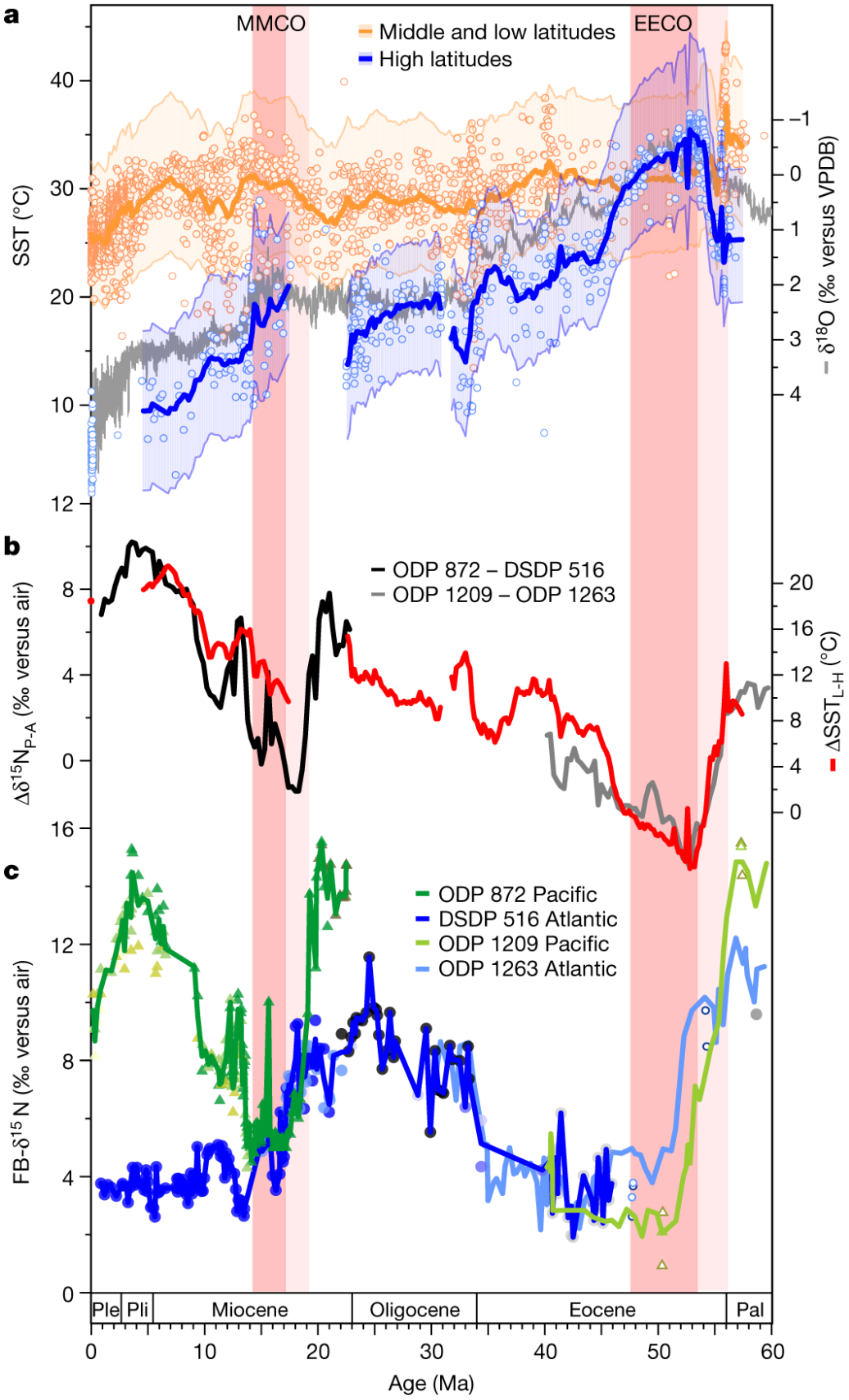

Figure 2. Evolution of FB-δ^{15}N and climate over the Cenozoic. a, Compilation of new and

previously published SST data based on the TEX_{86} palaeothermometer, divided into high latitudes (above 50° N/S) and low/middle latitudes (0–40° N/S), with LOESS smoothing (factor 0.02) and 90% confidence interval (see Methods and Supplementary Data 2). TEX_{86} temperature estimates are based on the BAYSPAR calibration (see Methods). The grey line shows the benthic foraminiferal oxygen isotope ratio ($\delta^{18}O$) compilation by Westerhold et al.8. b, $\Delta\delta^{15}N$P-A is the FB-$\delta^{15}N$ difference between Pacific ODP Site 872 and Atlantic DSDP Site 516 (black line) or between Pacific ODP Site 1209 and Atlantic ODP Site 1263 (grey line). ΔSSTL-H (red line) is the SST difference between low/middle latitudes and high latitudes (from a; the propagated 90% confidence interval for ΔSSTL-H is shown in Extended Data Fig. 4b). c, Average of species-specific FB-$\delta^{15}N$ from ODP Site 872 (green) and DSDP Site 516 (blue), together with mixed-taxa FB-$\delta^{15}N$ from ODP Site 1209 (light green) and ODP Site 1263 (light blue), calculated as the average of the two size fractions. Triangles and circles of different colours indicate individual species-specific or genus-specific FB-$\delta^{15}N$ in Site 872/1209 and Site 516/1263, respectively (see Extended Data Fig. 1 for details). Light pink bars indicate the first signs of global warming into the EECO and the MMCO, and darker bars indicate the main warm intervals, based on the benthic foraminifer $\delta^{18}O$ (a). Ple, Pleistocene; Pli, Pliocene; Pal, Palaeocene.

10. 晚中新世塔里木沙漠的湿润与偏心率极小值和东亚季风减弱有关

翻译人：夏文月 122310722@mail.sustech.edu.cn

Nie J, Wang W, Heermance R, et al. ***Late Miocene Tarim desert wetting linked with eccentricity minimum and East Asian monsoon weakening[J].*** *Nature Communications, 2022,13(1)*

https://doi.org/10.1038/s41467-022-31577-w

摘要：周期性的湿润是许多边缘地区沙漠的固有特征。先前的研究一致表明，在地球的高轨道偏心率和强夏季风时期，沙漠变得湿润。我们报告了中国北部的塔里木盆地西北部的晚中新世地层在地球低轨道偏心率期间沙漠湿润的第一个证据，这通常被认为超过了亚洲季风降水的范围。以现代塔里木湿润机制作为类比，我们提出东亚夏季风的减弱增强了向西的水汽输送，并且导致沙漠湿润模式与季风边缘地区沙漠湿润模式相反。我们的模型模拟支持这种推论。这一结果对于理解未来几千年在高大气 CO_2 含量和低偏心率下的非季风沙漠的环境变化具有深远的意义。

ABSTRACT: Periodic wetting is an inherent feature of many monsoon marginal region deserts. Previous studies consistently demonstrate desert wetting during times of Earth's high orbital eccentricity and strong summer monsoon. Here we report the first evidence demonstrating desert wetting during Earth's low orbital eccentricity from the late Miocene strata of the northwestern Tarim Basin of northern China, which is commonly thought to be beyond the range of Asian monsoon precipitation. Using mechanisms for modern Tarim wetting as analogs, we propose that East Asian summer monsoon weakening enhanced westward moisture transport and caused opposite desert wetting pattern to that observed in monsoon marginal region deserts. This inference is supported by our model simulations. This result has far-reaching implications for understanding environmental variations in non-monsoonal deserts in the next few thousands of years under high atmospheric CO_2 content and low eccentricity.

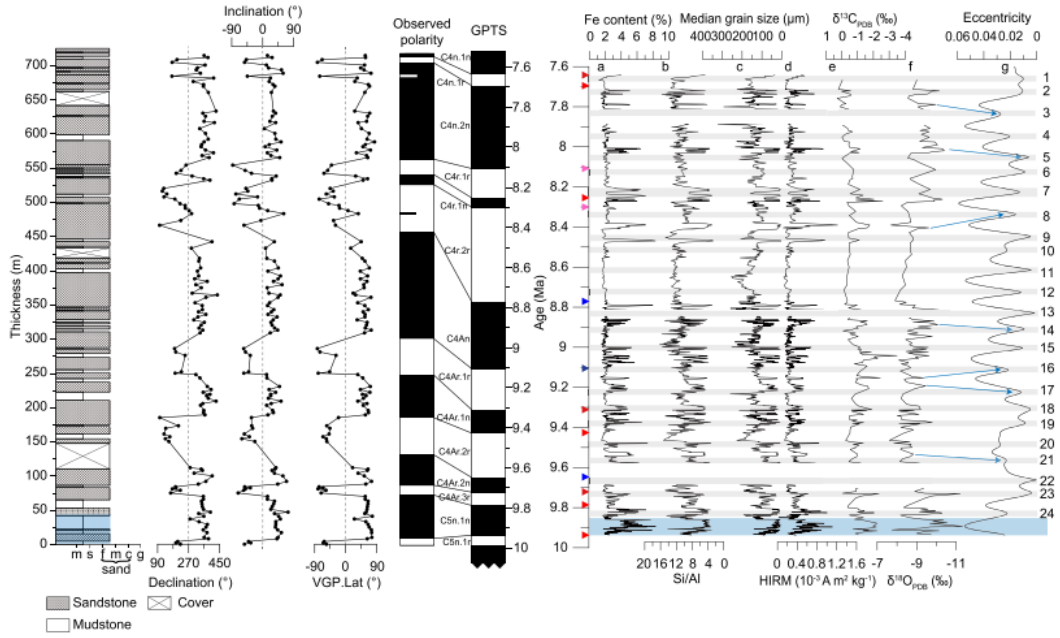

Figure 1. Lithology, age model, and paleoenvironmental proxy records from the studied section. The left panel shows the lithology and paleomagnetic age model. The right panel shows paleoenvironmental proxy records. a Fe content. b Si/Al. c Median grain size. d HIRM. e δ^{13}CPDB. f δ^{18}OPDB. g Eccentricity. Gray bars show the disappearance of eolian dune strata during low eccentricity. The blue shadow highlight dominant wet environment over the lower ~50 m of the strata. The triangles show reversals recorded by this section, with red, purple, and blue ones corresponding to tightly (<20 kyr), mediumly (35–40 kyr), and loosely (75–125 kyr) constrained reversals, respectively. Numbers on the right indicate eccentricity lows from top to bottom.

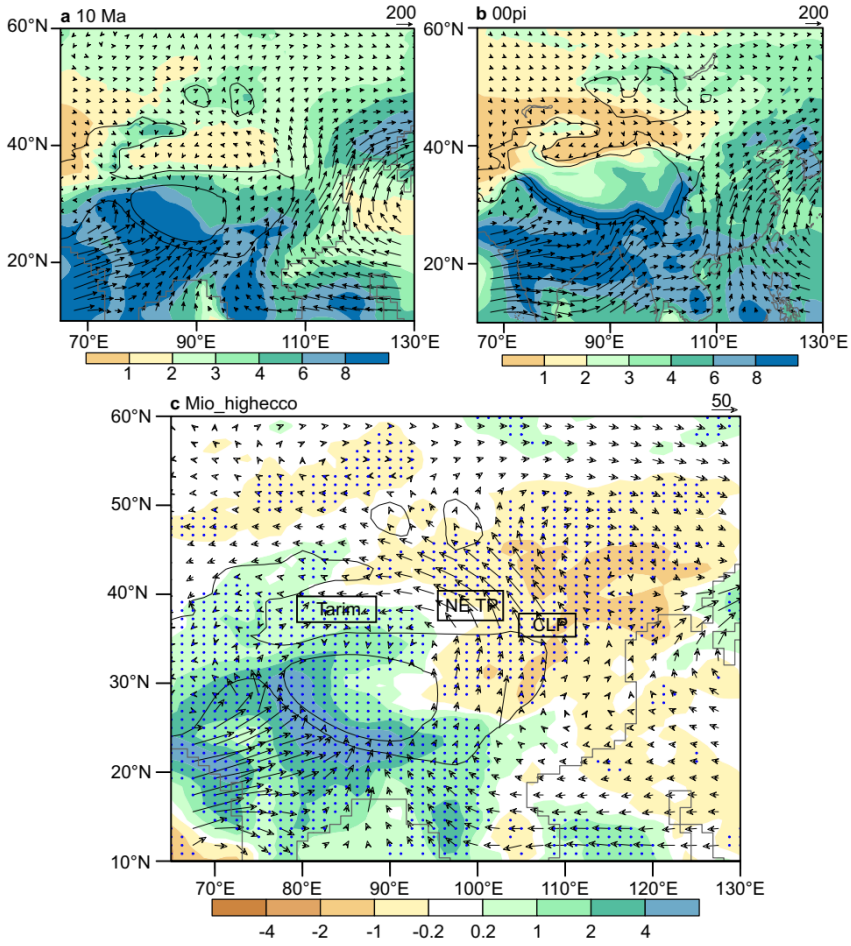

Figure 2. Simulated summer (JJA) precipitation (shaded, mm day^{-1}) and water vapor transport integrated from the surface to 700 hPa (vector, units: kg m^{-1} s^{-1}). JJA June, July and August. a Results using 10 Ma background boundary conditions and orbital parameters for 1950. b Results using preindustrial background boundaries and orbital parameters for 1950. c Precipitation and water vapor transport differences when increasing eccentricity from 0.01672 (year 1950) to 0.05. The difference is calculated by subtracting the high eccentricity results from the low eccentricity results. Green (yellow) color indicates more precipitation under lower (higher) eccentricity. Topography levels equal to 1500 m and 3000 m are highlighted with gray contours. The three black rectangles in c represent the rough locations of the Tarim Basin, Northeastern (NE) Tibetan Plateau (TP) and the Chinese Loess Plateau (CLP). Dotted regions indicate differences that are significant at the 90% confidence level.

11. 全球变暖使大西洋热带辐合带极端波动增加

翻译人：刘宇星 12232205@mail.sustech.edu.cn

Yi Liu, Wenju Cai, et al. ***Increased extreme swings of Atlantic intertropical convergence zone in a warming climate*** *[J]. Nature Climate Change, 2022: 1038.*

https://doi.org/10.1038/s41558-022-01445-y

摘要：大西洋热带辐合带（ITCZ）的年际变率影响大西洋沿岸国家的水文循环、极端天气事件、生态系统、农业和生活。它可能会经历年际极端波动，在北方春季向北移动数百公里，导致亚马逊中东部严重干旱和南美洲北部洪水。它的年际变率将如何响应全球变暖仍然未知。使用最先进的气候模型，我们预测在高碳排放情况下，极端北向波动将增加一倍以上。这种事件从 20 世纪每 20.4 年一次增加到 21 世纪每 9.3 年一次，其频率增加是由海面温度的平均状态变化支撑的，且赤道以北变暖速度更快。由于 ITCZ 随最高海面温度变化，所以其变暖的差异有助于增加极端波动的频率。我们的发现表明在大西洋沿岸国家，ITCZ 摆动引起的严重干旱/洪水大幅增加。

ABSTRACT: Interannual variability of the Atlantic intertropical convergence zone (ITCZ) affects hydrological cycles, extreme weather events, ecosystems, agriculture and livelihoods in Atlantic-rim countries. It can experience an interannual extreme swing, moving hundreds of kilometres northwards during boreal spring, causing severe droughts in central-eastern Amazon and floods in northern South America. How its interannual variability will respond to global warming remains unknown. Here using state-of-the-art climate models under a high-emission scenario, we project a more-than-doubling increase of extreme northward swings. This increase from one event per 20.4 years in the twentieth century to one per 9.3 years in the twenty-first century is underpinned by a mean state change of sea surface temperature, with faster warming north of the Equator. The warming differential facilitates the increased frequency of extreme swings, as the ITCZ follows the maximum sea surface temperature. Our finding suggests a substantial increase in ITCZ swing-induced severe droughts/floods in the Atlantic-rim countries.

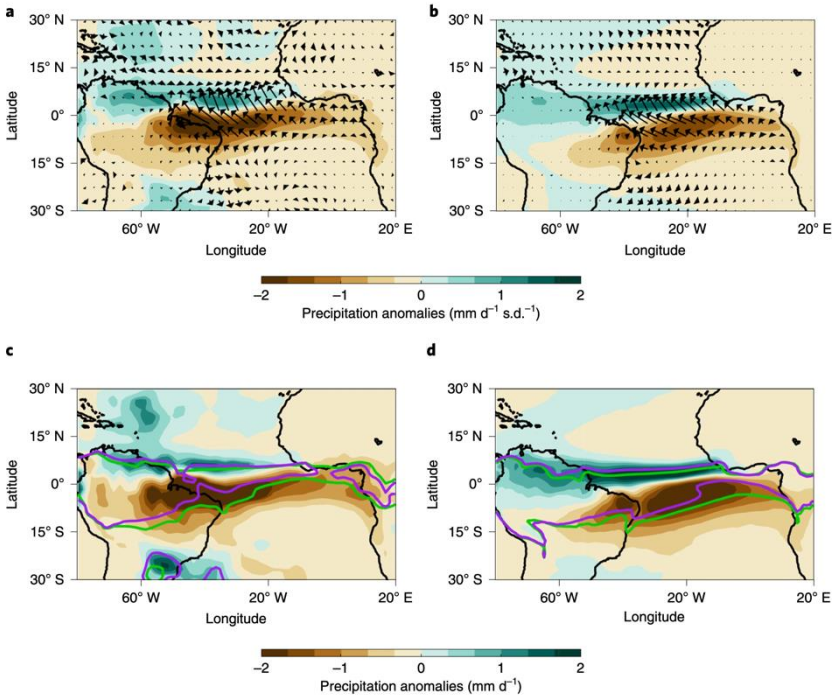

Figure 1. Meridional swings of Atlantic ITCZ in the observations and CMIP6 multimodel ensemble. a, MAM-averaged precipitation (mm d^{-1}, color shading) and surface wind (m s^{-1}, vectors) anomalies regressed onto the PC1 of EOF mode of MAM-averaged precipitation anomalies over the intertropical Atlantic domain (80° W-20° E, 20° S-20° N) during the 1982-2020 period in the observations (Data). b, Same as a but for the ensemble mean of 29 selected CMIP6 models over the entire 200 yr period. c, Composite of MAM-averaged precipitation anomalies (mm d^{-1}, color shading) over the 1983 extreme northward swing event and six moderate northward swing events (1990, 1992, 1993, 1998, 2010 and 2012) in the observations. Green and purple lines indicate the 5 mm precipitation contours of climatology during those extreme and moderate events, respectively. d, Same as c, but for the ensemble mean of 29 selected CMIP6 models over the entire 200 yr period. The 29 selected CMIP6 models simulate the observed tropical Atlantic precipitation EOF mode and the associated meridional swings of the Atlantic ITCZ, and capture the observed northward displacement of the rain band and associated precipitation anomaly pattern.

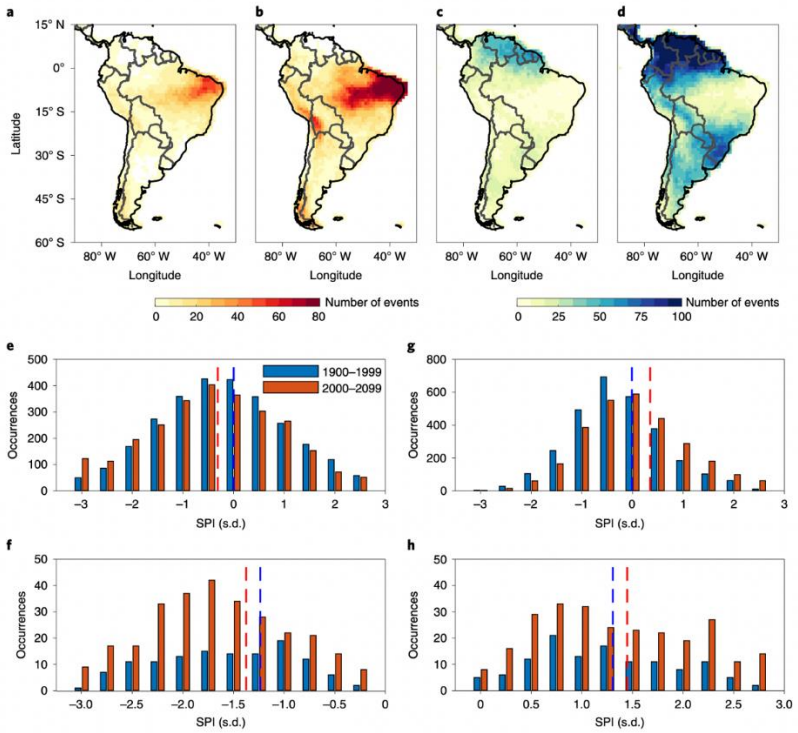

Figure 2. Extreme swing-induced meteorological droughts/floods in most-affected regions. a,b, Multimodel ensemble occurrences of meteorological dry events (SPI < -1.5) over South America that co-occur with extreme northward swing events during the twentieth century (a) and the twenty-first century (b). Here the SPI is a precipitation-based normalized index for defining meteorological drought/flood events (Standardized precipitation index and meteorological dry/wet events). c,d, Same as a,b but for occurrences of meteorological wet events (SPI > 1.5) during the twentieth century (c) and the twenty-first century (d). e,f, Multimodel ensemble histogram of the SPI over northeast Brazil (45° W-35° W, 8° S-4° S) during the twentieth century (blue bars) and twenty-first century (red bars) for all samples (e) and for extreme northward swing events only (f). Samples of each period are separated into 0.5 s.d. bins for all samples and 0.25 s.d. bins for extreme swing events only. The ensemble means of each period are indicated with blue and red dashed lines, respectively. g,h, Same as e,f but for the SPI over northern South America (75° W-60° W, 3° N-10° N) for all samples (g) and for extreme northward swing events only (h). The two histograms in e-h are statistically different above the 95% confidence level by a two-tailed Student's t test. The increased frequency of extreme swing events causes more extreme droughts/floods over the affected regions in South America.

12. 阿拉伯东南部全新世和更新世洞穴化石中记录的水分和季节变化

翻译人：聂美娟 12232216@mail.sustech.edu.cn

Fleitmann D, Burns S J, Matter A, et al. ***Moisture and seasonality shifts recorded in Holocene and Pleistocene speleothems from southeastern Arabia [J].*** *Geophysical Research Letters, 49, e2021GL097255.*

https://doi.org/10.1029/2021GL097255

摘要：在全新世早期到中期以及之前的湿润时期，阿拉伯南部地区的降雨来源和季节是有争议的，因为古湖泊沉积物只提供了关于降雨量的间接信息。关于阿曼北部霍提洞全新世和更新世石笋中流体包裹体水的氢、氧同位素测定是古降水同位素组成的直接指示。在间冰期高峰时期形成的流体包裹体的同位素值沿着季风水线绘制，指示南部季风水分来源。在此之前，季风主导的最后一段时间为距今约 10100 年至 6300 年，但在阿拉伯东南部的几十年间就结束了。随后降雨量的减少和夏季降水为主向冬季降水为主的变化对该地区人类群落产生了深刻的影响，并引发了内陆向资源较为丰富的沿海地区的迁移。

ABSTRACT: The source and seasonality of rainfall in southern Arabia during the early- to mid-Holocene and preceding humid periods are controversial because fossil lacustrine sediments provide solely indirect information on the amount of rainfall. Hydrogen and oxygen isotope measurements on fluid inclusion water trapped in Holocene and Pleistocene stalagmites from Hoti Cave in Northern Oman are direct indicators of the isotopic composition of paleoprecipitation. Isotope values of fluid inclusions formed during peak interglacial periods plot along monsoonal water lines and are indicative of a southern monsoonal moisture source. The last monsoon-dominated period lasting from ~10,100 to 6,300 years before present was terminated within a few decades in southeastern Arabia. The subsequent reduction in rainfall amount and change from predominantly summer to predominantly winter rainfall had a profound impact on human communities living in this area and triggered migration from inland to coastal areas where resources were more abundant.

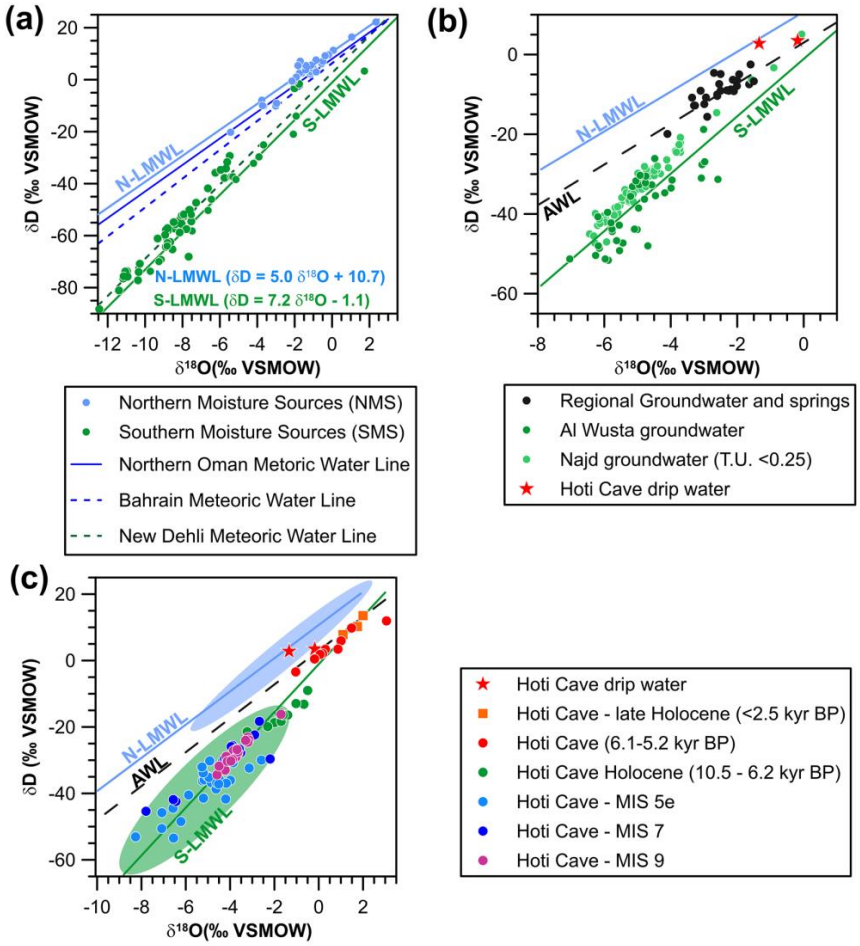

Figure 1. δ^2H and $\delta^{18}O$ values of rainfall, groundwater, cave drip, and fluid inclusion waters from south-eastern Arabia. (a) Modern rainfall samples from Oman (Macumber et al., 1994; Matter et al., 2006; Müller et al., 2019; Weyhenmeyer et al., 2000, 2002). Dots denote individual rainfall events from a northern (blue dots) and southern (green dots) moisture source. Also shown are the two Local Meteoric Water Lines (LMWL) characterizing rainfall originating from a northern LMWL and southern LMWL moisture source in Northern Oman. Northern Oman Meteoric Water Line ($\delta^2H = 5.1\ \delta^{18}O + 8$; Macumber et al., 1997). Dashed lines denote the meteoric water lines for Bahrain ($\delta^2H = 5.5\ \delta^{18}O + 6$; Gat et al., 2001) and New Delhi ($\delta^2H = 7.15\ \delta^{18}O + 2.6$; Pang et al., 2004). (b) Isotopic composition of groundwater from the area around Hoti Cave and cave drip water values (Matter et al., 2006). Also shown are groundwater values from Al Wusta and Najd which were recharged by rainfall from a southern moisture source (SMS). The black dashed line denotes the Akhdar Water Line ($\delta^2H = 5.1\ \delta^{18}O + 3$; Macumber et al., 1997). (c) Isotope composition of fluid inclusion waters extracted from Hoti Cave stalagmites from

different MIS. Blue and green shaded areas show the isotopic range of modern rainfall originating from a northern moisture source and SMS.

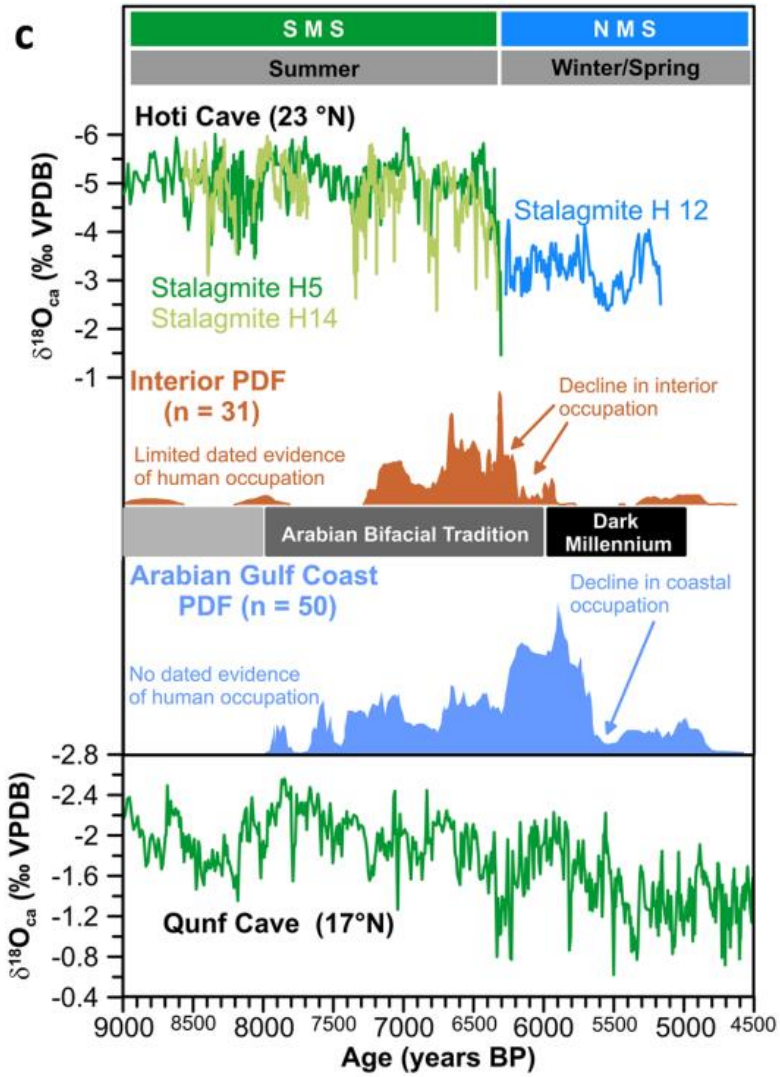

Figure 2. Images of the top of stalagmite H5 and comparison of the Hoti and Qunf Cave isotope records with archeological data from south-eastern Arabia. (a) Image of a polished section of stalagmite H5 and (b) cross polarized thin section image of the uppermost part (the black square in panel (a)). (c) Comparison of the Hoti and Qunf Cave $\delta^{18}O_{ca}$ records with summed probability distribution of ^{14}C dates and archeological periods from south-eastern Arabia (Preston et al., 2015).